Optical and vibrational properties of Be-Zn chalcogenide alloys and superlattices

Devki N. Talwar*
Department of Physics, Indiana University of Pennsylvania, 975 Oakland Avenue, 56 Weyandt Hall, Indiana, Pennsylvania 15705-1087, USA

(Received 22 April 2010; revised manuscript received 23 June 2010; published 26 August 2010)

The results of a comprehensive theoretical study for the optical and vibrational behavior of Be-Zn chalcogenide alloys and superlattices (SLs) are presented using a realistic lattice dynamical approach. Raman-scattering data for the zone-center optical modes and the results from first-principles calculations for the elastic, lattice constants, and critical-point phonons are employed in constructing an optimized second-neighbor rigid-ion model for BeS, BeSe, and BeTe. A simple explanation is provided for the unusual characteristics of the optical phonon dispersions found in Be chalcogenides, alloys and $(BeSe)_m/(ZnSe)_n$ SLs compared to those of many other Zn-based II-VI compound semiconductors. An elastic continuum model has offered a strong corroboration to the observed doublets by Raman spectroscopy in the BeTe/ZnSe superlattices near 25–30 cm^{-1} as the folded LA modes due to mini-zone folding in the $z(xx)\bar{z}$ scattering geometry. By using a standard methodology of multilayer optics with appropriate alloy dielectric functions, we have analyzed the IR reflectance spectra of BeZnSe/GaAs thin epilayers at an oblique incidence with a three-oscillator model. Comparison of our results with the reflectivity data has provided a strong validation to the fact that in the ~400–575 cm^{-1} frequency region there exist at least two types of Be-Se bonds with optical modes involving two kinds of local atomic arrangements.

DOI: 10.1103/PhysRevB.82.085207 PACS number(s): 78.20.−e, 63.20.Pw, 63.20.D−

I. INTRODUCTION

Understanding the basic properties of wide band-gap Be-Zn chalcogenides, their alloys and superlattices (SLs), are currently of great academic and technological interest[1–5] from the designing of novel materials to the fabrication of nanoelectronic and photonic devices. In recent years blue-green laser diodes (LDs), optical modulators, photodetectors, wave guides, and sensors operating in the visible to ultraviolet spectral range were developed[6–10] from II-VI-based alloys and compositionally modulated heterostructures. The development of such devices was driven largely by the higher demand for the information density in the optical data storage systems. In the mid 90's ZnSe (Refs. 11–15) was the only material used for generating light in the 460–540 nm wavelength range. However, the success in the development of blue-green lasers remained limited by the relatively short lifetime caused by various unknown defects[16–21] in the alloys of ZnSe-related heterostructures. A renewed interest in the II-VI-based material systems arose[22–27] recently when a partial substitution of Zn by Be in Zn(Mg)Se and Zn(Mg)Te not only improved the fundamental properties but also resulted in a significant increase in the covalent bonding, higher cohesive energy, larger band gap, and higher *p*-type dopability in these alloys. For instance, by varying the composition (x,y) in $Be_xMg_yZn_{1-x-y}Se$ has allowed one to grow thin films of quaternary compounds perfectly lattice matched[28,29] to GaAs (001). Such thin films can be used to tailor both optical and electronic properties over a wide energy range. In BeZnSe(Te) alloys, besides tuning the fundamental band gap and the dielectric function in broad limits, the coexistence of strongly ionic and strongly covalent bonds[22] in the same crystalline material have made its elastic and dynamical properties even more interesting. Again, the concomitant increase in the bond strength of Be compounds is expected to have significant influence on the defect generation and propagation. Although Be chalcogenides are projected to be the better materials for optoelectronic devices than the sulfur-based alloys, there is not much information available currently about the doping, stacking fault formation, reduction of the defect propagation, etc. If these materials are to be used as cladding layer, guiding, and *p*-type contact layer in LDs, the knowledge of defect structures causing deep traps is very crucial, as the presence of such defects could adversely affect the quantum efficiency of the photonic devices. In other words, the increasing complexity of the novel Be-Zn-based chalcogenides, alloys, quantum wells, and SLs grown by epitaxial techniques have created the urgent need for material characterization by using powerful optical techniques.

Among many experimental methods, the spectroscopic ellipsometry[30–34] is a very well-established nondestructive technique for investigating the optical properties, especially the complex dielectric function $\tilde{\varepsilon}(\omega)[=\varepsilon_1(\omega)+i\varepsilon_2(\omega)]$ in bulk semiconductor materials as well as thin films. Ellipsometry has the distinct advantage over the reflectivity and transmission methods for determining $\tilde{\varepsilon}(\omega)$ without having to perform the Kramers-Krönig transformations. Exhaustive ellipsometry measurement[30–34] in $Zn_{1-x}Be_xSe$ ($Zn_{1-x}Be_xTe$) has provided the extended electronic structure of the alloy system revealing BeSe (BeTe) to be an indirect band-gap material. The direct-to-indirect transition occurs at $x=0.46$ ($x=0.28$) in the alloy as deduced from the combined photoluminescence-reflectivity analysis.[35,36] First-principles pseudopotential calculations[37–44] have been used to investigate structural, elastic, and electronic properties of the zinc-blende phase of Be chalcogenide materials. Unfortunately, very limited information exists on the vibrational and thermodynamic properties[45–47] of Be-Zn chalcogenides. For instance, the Debye temperature θ_D is a fundamental physical property used to distinguish between the high- and low-temperature regions of any material. If $T>\theta_D$ one expects all phonon modes to have energy k_BT, and if $T<\theta_D$ we expect high-frequency modes to be frozen. In the absence of experimental results on the thermodynamic properties a few theo-

retical attempts have been made recently. The lattice dynamics study of BeSe and BeTe reported earlier by Doyen-Lang *et al.*[45] have used a simplified phenomenological De Launay[48] model with two (central and angular) force constants. Wagner *et al.*[46,47] calculated the zone-center TO phonon values for BeSe and BeTe by using first-principles calculations, based on frozen-phonon approximation within the pseudopotential scheme and the density-functional theory (DFT). More recently, first-principles studies of the structural, electronic, and dynamical properties of Be chalcogenides were performed[39] using the plane-wave pseudopotential (PP) method within the density-functional theory.

One must note that an accurate description of the vibrational and thermodynamic behavior of semiconductor materials plays a crucial role in the determination of their diverse physical properties such as phase transitions, and electron-phonon interactions, etc. Many other interesting characteristics, such as electronic transport and nonradiative electron relaxation processes, required for device design and engineering are strongly influenced by the phonon modes as well. Lattice dynamics being the source of important elementary excitations has been commonly used in the standard materials characterization by using Raman-scattering spectroscopy,[7,49–57] ellipsometry,[30–34] and/or infrared (IR) reflectivity[32,33] studies. The inelastic neutron-scattering experiment, the most efficient method to reveal the normal modes in bulk materials [e.g., ZnS,[58] ZnSe,[59] and ZnTe (Ref. 58)] has not been applied to the lattice dynamics of Be chalcogenides. Again, the neutron-scattering method cannot be used for studying the vibrational properties of thin films or nanostructured materials (viz., SLs or quantum wells, etc.) because the available epitaxially grown samples are too lean to obtain measurable signals to resolve modes and branches of the phonon dispersions lying very close in frequency. In Be chalcogenide $Be_xZn_{1-x}(Mg_{1-x})Se(Te)$ alloys although significant amount of Raman-scattering spectroscopy,[7,49–57] ellipsometry,[30–34] and IR reflectivity data[32,33] exist in the literature on the vibrational properties and a few theoretical calculations attempted,[45–47] the results, however, differ considerably.

It is worth mentioning that in most ternary $A_xB_{1-x}C$ compound semiconductors the "cation-anion" bond lengths (d_{AC}, d_{BC}) are generally conserved over the entire composition range x, i.e., the values of d_{AC} and d_{BC} are retained in the parent binary (AC, BC) compounds. This simplest intuitive picture suggests that at any given x all the d_{AC} and d_{BC} bonds are equivalent and immersed into the same uniform continuum whose physical properties are locally averaged according to the virtual crystal approximation (VCA). The bond-length distribution in this configuration is referred[49] to as the 1-bond→1-mode type and its optical phonon modes can be described in terms of a modified random element isodisplacement (MREI) model. In certain alloy systems where the sizes of the anions and cations are radically different one might suspect that preserving the cation-anion bond lengths become increasingly difficult which, in turn, would considerably affect the phonon behavior of the ternary alloys. In addition to the small size, the light mass of Be is expected to cause atypical phonon properties of Be chalcogenide alloys[7,49–57] and SLs compared to the Zn-based II-VI compound semiconductors of similar crystal structure. Consequently, one would anticipate new phonon features to occur in $(BeX)_m/(ZnY)_n$ SLs (Refs. 56 and 60) (with X, Y=S, Se, and Te) such as folded acoustic phonons, confined optical modes and interface phonons, etc.

In this paper we have used a realistic lattice dynamical model[61–64] to undertake a comprehensive theoretical study (cf. Secs. II and III) of phonon properties in Be chalcogenides, their alloys and SLs and compared our results where possible with the existing experimental and/or theoretical data. The calculated results of phonons at critical points, one-phonon density of states, and Debye temperatures[43,44] agree very well with the first-principles theoretical and experimental [Raman scattering[7,49–57] and IR (Refs. 32 and 33)] data. In contrast to the Zn-based materials, our lattice dynamical results of phonon dispersions in Be chalcogenides exhibited rather unusual behavior. An explanation for these peculiarities is provided after comparing the results of phonons with B pnictides[62] and group III-Ns (Ref. 63) by correlating them to the large mass difference between Be and chalcogen atoms as well as to the decrease in the bond polarity. An elastic continuum model[65] (cf. Sec. III) is adopted here to describe the long-wavelength acoustic phonons, zone-folding effects, and the creation of mini gaps in SLs. Realistic calculations are carried out of the phonon behavior for the zone-center optical modes in $(BeSe)_m/(ZnSe)_n$ (m=n for 2 and 3) SLs as a function of θ (cf. Sec. IV B). In a periodic $(BeTe)_m/(ZnSe)_n$ SLs the calculated results for the folded acoustic phonons (FAPs) including modes splitting at the center and at the edge of the SL-Brillouin zone (BZ) are compared with the existing Raman-scattering[56] data (cf. Sec. IV C). In terms of a MREI (Ref. 64) model the zone-center ($\vec{q}$=0) LO and TO phonons for the ternary $Be_xZn_{1-x}(Mg_{1-x})Se(Te)$ alloys are shown qualitatively to exhibit, at first sight, a typical two-mode behavior[56] (cf. Sec. IV D) for a wide composition range. As the Be content in $Be_xZn_{1-x}Se(Te)$ ternary alloy increases above a critical value x_c additional well-resolved doublets related uniquely to Be-Se (Be-Te) type phonons are detected in Raman-scattering experiments.[7,42–57] Of particular interest are the TO modes as they consist of quasi-independent oscillators exhibiting 1-bond→2-mode behavior in the percolation scheme.[7,42–57] In $Be_xZn_{1-x}Se(Te)$ alloys this atypical phonon mode behavior is explained recently by Pagès *et al.*[49] by using a double-branch percolation model which discriminates between vibrations within the randomly formed hard Be-rich host region and the soft Zn-rich region. Here we have used a traditional formulation of the multilayer[66] optics with appropriate alloy dielectric functions and calculated the IR reflectance spectra of thin $Be_xZn_{1-x}Se/GaAs(001)$ epilayer at an oblique incidence (cf. Sec. IV E) within a three-oscillator model. Our analysis of the IR reflectivity spectra for $Be_xZn_{1-x}Se$ ternary alloy system has provided a strong corroboration to the fact that in the frequency range of 400–575 cm^{-1} there exist at least two types of Be-Se bonds with optical modes involving two kinds of local atomic arrangements (ordering). Theoretical results are compared and discussed with the existing experimental data in Sec. IV and concluding remarks are presented in Sec. V.

II. THEORY

In several II-VI (ZnS, ZnSe, ZnTe, and CdTe) zinc-blende-type materials, the existing inelastic neutron-scattering data of phonon dispersions[58,59] have already provided us with a very good description of their interatomic forces. In Be chalcogenides, although significant amount of Raman[7,49–57] and IR data[32,33] on the vibrational properties exist in the literature and a few theoretical studies attempted,[45–47] the complete description of lattice dynamics is, however, still rather scarce. Again, despite the existence of limited experimental data on $(BeTe)_m/(ZnSe)_n$, the dynamical behavior of isoanion $(BeSe)_m/(ZnSe)_n$ SLs has not been adequately investigated either experimentally or theoretically.

One must note that in extracting the dynamical properties of solids, there exist two important methodologies: (a) *microscopic analysis*[67,68] which starts with an ionic potential screened by the electron gas in deriving the structural properties and (b) macroscopic analysis[61,69–74] which uses phenomenological models in terms of general interatomic forces and consequently explaining the physical features of the material system. In the former case there are only a limited numbers of *ab initio* studies available[39] that cover the structural, electronic, and dynamical behavior of the Be-Zn (Refs. 45–47) chalcogenides. The vibrational properties of defects in BeS, BeSe, and BeTe have not yet been treated through first-principles calculations, and for the majority of II-VI materials the available results by the Green's function theory[69] use the *macroscopic methods*. In either scheme, the most important point that compels recognition to a lattice dynamical method demands simultaneously correct eigenvalues and eigenvectors. Although the impetus for examining the phenomenological models comes from *ab initio* methods, the later approaches have not yet replaced the former schemes completely. The simple reason is that the microscopic methods, in general, deal only with phonons at a few high-symmetry points while the efficiency of macroscopic models comes to profit when different Brillouin zone averages are evaluated, viz., in the calculations of Green's functions used for studying the impurity vibrations.[69] Our earlier investigations of localized vibrational modes for identifying the microscopic lattice structures of silicon impurities in $Ga_{1-x}Al_xAs$ alloys for low Al composition (x) has provided us an indirect support for the reliability of the calculated phonons for GaAs and AlAs using rigid-ion model. The same model was also applied successfully for understanding the pressure-dependent properties of II-VI (Ref. 74) compounds by correlating the phonon modes with the stiffeness of the bonds under external stimulus (pressure) for analyzing the thermal-expansion coefficients and mode Grüneisen constants. Thus, from the support of earlier successful calculations in many II-VI and III-V compound semiconductors of similar crystal structure, we strongly believe that our macroscopic approach is just as reliable and has a very high potential of predicting the lattice dynamical properties for the bulk Be-Zn chalcogenide materials and their superlattice structures.

A. Phonons in bulk cubic Be-Zn chalcogenides

To the best of our knowledge, there exist no neutron-scattering data of phonon dispersions in Be chalcogenides. The main reason for the lack of information for the lattice dynamics in BeS, BeSe, and BeTe is the fact that single crystals large enough for inelastic neutron-scattering studies are not available and most of the accessible epifilms that exist are grown very thin by using the molecular-beam epitaxial (MBE) technique. In Be chalcogenides, despite the lack of complete information for the lattice dynamics at all $\vec{q}$'s within the Brillouin zone, the *first-order* Raman scattering[7,49–57] and IR spectroscopy[32,33] offered valuable data at least for the phonon energies near $\vec{q} \approx 0$. The imposed restriction of the conservation of $\vec{q} \approx 0$ in optical spectroscopy is a direct consequence of the existence of the lattice of translations as symmetry elements. To circumvent this restriction, it is possible to remove the translational symmetry operations by making the material samples either (i) microcrystalline (ii) introduce impurities, (iii) fabricate artificial SL structures, and/or (iv) study the *second-order* spectra.

In addition to the frequencies at Γ critical points from the first-order optical spectroscopy[7,49–57] calculations of phonon energies at high-symmetry points (Γ,X,L) and the values of the first-order elastic constants[37] are available for BeS, BeSe, and BeTe from the *ab initio* total-energy pseudopotential methods[38,39] within the local-density approximation (LDA). This information has been very important to us in constructing the second-neighbor rigid-ion model, for describing the lattice dynamical properties[61] of Be chalcogenides (cf. Sec. IV A). It is worth mentioning that the rigid-ion model incorporates both the long-range Coulomb forces in terms of an effective charge (Z_{eff}) and short-range forces [nearest (A,B) and next nearest (C_i, D_i, E_i, and F_i, with $i=1,2$)] up to an including second neighbors. The force constants for BeS, BeSe, and BeTe are optimized (see Table I) by using a nonlinear least-square fitting method with constrained parameters and weighting to the existing information of the phonon modes[7,49–57] at critical points, elastic and lattice constants[37–39] (see Table II).

B. Phonons in $(BeSe)_m/(ZnSe)_n$ SLs

We have performed extensive rigid-ion model calculations to understand the lattice dynamical properties of $(BeSe)_m/(ZnSe)_n$ SLs. Our approach is based on the generalization of the host crystal phonons[70] and uses force parameters between the host lattice atoms as well as the dynamic effective charges taken over from the bulk materials. This study yields phonon-dispersion relations in SLs for any arbitrary direction of $\vec{q}$, i.e., for finite q_x, q_y, and q_z—allowing us to have a complete assessment of the vibrational features including the propagating modes, confined and interfacing phonons. We have carried out calculations about the angular dependence of phonons along [001] direction in $(BeSe)_m/(ZnSe)_n$ SL with wave vectors parallel and perpendicular to the z direction following the procedure described in Ref. 70. Before presenting the results of phonons (cf. Secs. IV B and IV C) in SLs we would like to summarize here the salient features based on simple group theoretical arguments.

In $(BeSe)_m/(ZnSe)_n$ SL, the periodicity along the [001] direction induces (i) the lowering of crystal point-group sym-

TABLE I. Optimized set of rigid-ion model parameters (10^5 dyn/cm) for the lattice dynamics of Be chalcogenides.

Model parameters[a]	BeS	BeSe	BeTe
A	−0.36306	−0.333	−0.2802
B	−0.295	−0.26	−0.25
C_1	−0.034	−0.018	−0.009
C_2	−0.0635	−0.089	−0.045
D_1	−0.02125	−0.0019	−0.0057
D_2	−0.07800	−0.0704	−0.053
E_1	0.032	0.0165	0.0135
E_2	−0.081	−0.0792	−0.0624
F_1	−0.0028	−0.014	0.0044
F_2	0.0156	0.0719	−0.0361
Z_{eff}	0.6506	0.688	0.5489
a_o (Å)	4.865	5.139	5.627

[a]In the notations of Ref. 61.

metry from T_d to D_{2d} and (ii) the expansion of the primitive unit cell from 2 to $2(m+n)$ atoms. For the zone-center phonons, the symmetry is B_2 for the longitudinal and E for the doubly degenerate transverse modes. If the wave vector is parallel to the SL axis (z axis: direction Γ-Z), the point group of the wave vector is C_{2v} and the mode symmetries are A_1 for the longitudinal and B_1, B_2 for the transverse phonons. For wave vectors perpendicular to the SL axis (x axis: direction Γ-X) and for small $\vec{q}$'s ($|\vec{q}| \to 0$) forming an angle θ with the SL axis on the ZOX plane, the group of the wave vector is C_s and the zone-center B_2 modes transform into A' symmetry while the E modes split into A' and A'' modes. The A'' modes are transverse in nature with the ions vibrating along the OY direction. These modes have a constant frequency independent of angle θ. The A' modes, on the other hand, are of mixed polarization showing dispersion with the direction of the wave vector (or angle θ), especially the optical ones, due to the macroscopic field associated with them. Only the antisymmetric (odd-numbered) modes carry a macroscopic field, and this field vanishes for the symmetric (even-numbered) modes. Thus, only odd-numbered optical phonons show angular dispersions: the LO phonons decrease with the increase in $\vec{q}$ while TO phonons split, one showing no dispersion and the other exhibiting an upward dispersion. Again, whenever the phonon frequency approaches another mode with the same symmetry (odd numbered), the two modes mix with each other, resulting in an anticrossing behavior.

TABLE II. Relevant set of physical parameters for Be chalcogenides used in optimizing the rigid-ion model parameters (see Table II). The elastic constants c_{11}, c_{12}, and c_{44} are in 10^{11} dyn cm^{-2}; lattice constant in (Å) critical-point phonon frequencies are in wave number.

Physical parameters	BeS	BeSe	BeTe
c_{11}	18.4[a]	14.9[a]	11.1[a]
c_{12}	7.5[a]	5.9[a]	4.3[a]
c_{44}	9.9[a]	8.1[a]	6.0[a]
a_o	4.865[a]	5.139[a]	5.627[a]
LO(Γ)	647	556[b]	495[b]
TO(Γ)	562	498[b]	468[b]
LO(X)	652[b]	601[b]	540[b]
TO(X)	507[b]	451[b]	425[b]
LA(X)	364[b]	218[b]	159[b]
TA(X)	237[b]	139[b]	97[b]
LO(L)	607[b]	556[b]	504[b]
TO(L)	543[b]	485[b]	455[b]
LA(L)	362[b]	216[b]	158[b]
TA(L)	161[b]	99[b]	69[b]

[a]PP-LDA (plane-wave pseudopotential local-density approximation), Ref. 37.
[b]FP-DFT (first-principles density-functional theory), Ref. 39.

C. Multimode behavior of optical phonons in ternary alloys

In most of the compound semiconductor ternary $A_xB_{1-x}C$ alloys, the compositional dependence of zone-center optical phonons of their binary AC, BC compounds usually exhibit *one-*, *two-*, or *mixed-mode* behavior[71] depending upon the relative masses of the constituent atoms and their interatomic force constants. In the one-mode behavior, only one set of LO and TO phonons is seen varying linearly from one end member (AC for $x=1$) to the other (BC for $x=0$) with mode intensities remaining almost constant. In the two-mode behavior, the two sets of LO and TO optical phonons vary continuously from the end members and converge to the impurity modes (localized or gap) of the other end-members binaries' at the limiting values of the composition x, i.e., $B\underline{C}:A$ for $x \to 0$ and $A\underline{C}:B$ for $x \to 1$, respectively. In the Raman-scattering experiments of the two-mode behavior, each pair will correspond to a mode of one of the binary end members and its relative intensity is found approximately proportional to the fraction of the relevant constituent. In the mixed-mode behavior, the impurity mode lies within the reststrahlen band of a binary end member. In order to describe the two-mode behavior in $A_xB_{1-x}C$ alloys we have used an MREI model.[64] Within the framework of a VCA this MREI model is based on the description of mixed crystals, i.e., it assumes an ideal effective medium which is perfectly homogenous at the local region. The statistical average of the neighbors depends upon the composition x. The assumption of isodisplacement in the MREI scheme means that the cations as well as the anions of like species vibrate as rigid units, i.e., each unit vibrates with one phase and amplitude. With these assumptions the three equations of motion involving A, B, and C atoms in the $A_xB_{1-x}C$ alloy are solved requiring (i) the masses of the three atoms m_A, m_B, and m_C, (ii) force constants F_{AC0}, F_{BC0} of the end members as well as a force constant F_{AB0} between the second-neighbor atoms A-B, (iii) a parameter θ describing the variation of the force constants $\left[\frac{F_{AC}}{F_{AC0}} = \frac{F_{BC}}{F_{BC0}} = \frac{F_{AB}}{F_{AB0}} = 1 - \theta x\right]$ with composition x, (iv) high-frequency dielectric constants $\varepsilon_{\infty AC}$, $\varepsilon_{\infty BC}$, and (v) oscillator strengths $4\pi\rho_{AC}$ and $4\pi\rho_{BC}$. The six MREI model parameters are usually determined self-consistently by using

TABLE III. Parameters needed for optimizing the MREI model to calculate two-mode behavior in ternary alloys.

	BeSe	BeTe		ZnSe		ZnTe		MgSe	
ω_{TO} (cm^{-1})	496	461		205		176		237	
ω_{LO} (cm^{-1})	576	502		252		206		340	
ω_I (cm^{-1})	(BeSe:Zn)229 (BeSe:Mg)268	(BeTe:Zn)195		(ZnSe:Be)452		(ZnTe:Be)411		(MgSe:Be)509	
ε_∞	6.1	6.9		5.75		7.28		3.8	
a_o (Å)	5.152	5.625		5.6676		6.104		5.89	
m_{Be} (amu)	9.01	m_{Be} (amu)	9.01	m_{Zn} (amu)	65.38	m_{Zn} (amu)	65.38	m_{Mg} (amu)	24.31
m_{Se} (amu)	78.96	m_{Te} (amu)	127.6	m_{Se} (amu)	78.96	m_{Te} (amu)	127.6	m_{Se} (amu)	78.96

MREI model parameters[a]

$AB_{1-x}C_x$:($SeMg_{1-x}Be_x$) alloy		$AB_{1-x}C_x$:($SeZn_{1-x}Be_x$) alloy		$AB_{1-x}C_x$:($TeBe_{1-x}Zn_x$) alloy	
e^*_{AB}	1.08	e^*_{AB}	0.784	e^*_{AB}	0.48
e^*_{AC}	0.634	e^*_{AC}	0.634	e^*_{AC}	0.66
F_{AB0}	1.035×10^{05}	F_{AB0}	1.22×10^{05}	F_{AB0}	1.21×10^{05}
F_{AC0}	1.41×10^{05}	F_{AC0}	0.99×10^{05}	F_{AC0}	1.43×10^{05}
F_{BC0}	0.003×10^{05}	F_{BC0}	0.103×10^{05}	F_{BC0}	0.042×10^{05}
θ	−0.05	θ	−0.5	θ	0.28

[a]In the notations of Ref. 64.

the least-square fitting methods from the six phonon frequencies ω^{LO}_{AC}, ω^{TO}_{AC}, $\omega_{AC:B}$ and ω^{LO}_{BC}, ω^{TO}_{BC}, $\omega_{BC:A}$.

By using the MREI (Ref. 64) model parameters of Table III the zone-center ($\vec{q}=0$) LO and TO phonons for the ternary $Be_xZn_{1-x}(Mg_{1-x})Se(Te)$ alloys are *qualitatively* shown to exhibit, at first sight, a typical two-mode behavior (cf. Sec. IV D) for a wide composition range. One must note, however, that when the Be content in $Be_xZn_{1-x}Se(Te)$ is increased above a critical value x_c additional well-resolved doublets are observed[7,42–57] related to Be-Se (Be-Te) type phonons (cf. Sec. IV D) exhibiting 1-bond→2-mode type behavior. Such atypical phonon modes cannot be explicated by the MREI model. In $Be_xZn_{1-x}Se(Te)$ alloys the observed optical phonons are explained recently by Pagès *et al.*[49] using a double-branch percolation model which discriminates between vibrations within the randomly formed hard Be-rich host region and the soft Zn-rich region. It is worth mention here that the percolation model comes to describe a random mixed crystal as a composite rather than as a uniform continuum as represented in the VCA-based MREI scheme. In our study we have performed IR reflectivity calculations in $Be_xZn_{1-x}Se/GaAs(001)$ thin epilayer at oblique incidence in terms of a damped three-oscillator Lorentz model calculating the complex dielectric function $\tilde{\varepsilon}(\omega)$ and using the methodology of multilayer optics. Comparison of the results (cf. Sec. IV E) with experimental data has provided a strong corroboration to the fact that in the frequency range of 400–575 cm^{-1} there exist two types of Be-Se bonds with optical modes involving two types of local atomic arrangements (ordering).

III. FOLDED ACOUSTIC PHONONS IN SUPERLATTICES

In order to explain the folded acoustic phonons in SLs one can start by considering propagation of the elastic waves in the direction normal to the interface of a two layered, infinitely extended periodically structured SL (see Fig. 1). The dispersions of folded acoustic phonons including the splitting at the center and at the edge of the BZ of the SL are calculated within the elastic approximations in which the dispersion relations of the constituents are assumed to be linear, i.e.,

$$\omega^2 = q^2v^2 \quad \text{with} \quad v = \sqrt{\frac{C}{\rho}}, \tag{1}$$

where v, ρ, and C are the sound velocity, the mass density, and the elastic constants, respectively. Within the layers, the displacement u satisfies the one-dimensional wave equation

$$\rho_i \frac{\partial^2 u_i}{\partial t^2} = C_i \frac{\partial^2 u_i}{\partial z^2}, \tag{2}$$

where $u_i(z)$ is the atomic displacement of the corresponding material layer $i(=1,2)$. Our aim here is to solve these equa-

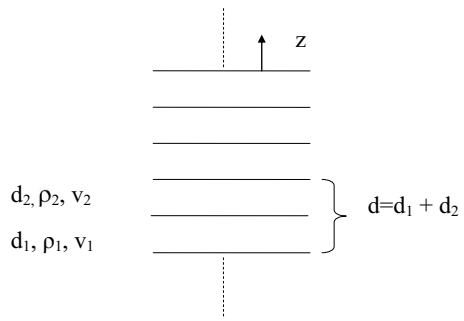

FIG. 1. A periodically structured infinite superlattice consisting of two types of layers per period d, each characterized by thickness d_i; density ρ_i; and sound velocity v_i $(i=1,2)$. The z axis is taken normal to the interfaces.

tions with boundary conditions that u and $C\frac{\partial u}{\partial z}$ are continuous at the interface, i.e.,

$$u_1(z_i) = u_2(z_i), \tag{3a}$$

$$C_1 \left.\frac{\partial u_1}{\partial z}\right|_{z=z_i} = C_2 \left.\frac{\partial u_2}{\partial z}\right|_{z=z_i}, \tag{3b}$$

and consider a wave of angular frequency ω so that $\frac{\partial^2 u}{\partial t^2} = -\omega^2 u$. One must note that Eq. (3a) expresses the continuity of the atomic displacements and Eq. (3b) expresses the continuity of stress at each interface. Again, as the SL structure has the translational period $d(=d_1+d_2)$ in the z direction, one can introduce the wave-vector component q by using the Bloch's theorem such that

$$u(z+d) = e^{iqd}u(z). \tag{4}$$

Consequently, the solution of the wave Eq. (2) in either medium (of material layer i in the nth period) will be a superposition of the plane wave propagating forwards and backwards modulated with a Bloch wave

$$u_{n,i}(z,t) = [a_i^+ e^{ik_i(z-d_i/2)} + a_i^- e^{-ik_i(z-d_i/2)}]e^{i(nq_z d-\omega t)} \tag{5}$$

with $k_i = \frac{\omega}{v_i}$ and q_z being the SL wave vector. Imposing the boundary conditions, i.e., Eqs. (3a) and (3b) at each interface and using Eq. (2) leads to a 4×4 secular determinant resulting in an explicit form of the dispersion equation[65]

$$\cos(q_z d) = \cos(k_1 d_1)\cos(k_2 d_2) - [(1+\zeta^2)/2\zeta]\sin(k_1 d_1)\sin(k_2 d_2), \tag{6}$$

where ζ is the ratio of the acoustic impedances of the two constituent bulk materials. For $\zeta = 1$, Eq. (6) becomes

$$\cos(q_z d) = \cos(k_1 d_1 + k_2 d_2) \tag{7}$$

with solutions

$$\omega\left(\frac{d_1}{v_1} + \frac{d_2}{v_2}\right) = \pm qd + n\pi. \tag{8}$$

Equation (8) corresponds to the folding of acoustic phonon-dispersion curves into the reduced zone as the layers are impedance matched and the medium effectively becomes continuous acoustically. For $\zeta \neq 1$ in Eq. (6) leads to a frequency splitting of the acoustic phonons both at the center $(q_z=0)$ as well as at the edge $(q_z=\frac{\pi}{d})$ of the SL BZ.

It has been demonstrated by Santos *et al.*[72] that the frequency gaps of the folded acoustic phonons can be calculated from the displacement field in Eq. (6) as the superposition of two plane waves travelling in opposite directions. The ratio of their amplitudes within the layer i (=1 and 2) $\frac{a_i^-}{a_i^+}$ can be given by

$$\frac{a_i^-}{a_i^+} = \pm\frac{1}{\varepsilon}\frac{\sin\left(\frac{\omega(t_2+t_1)-q_z d}{2}\right)}{\sin\left(\frac{\omega(t_2-t_1)-q_z d}{2}\right)} \quad \text{with} \quad \varepsilon = \frac{\zeta-1}{\zeta+1}, \tag{9}$$

where $t_i = d_i/v_i$ is the phase traversal time through layer i.

A. Zone-center gaps

The gaps of the folded acoustic phonons at the center of the Brillouin zone $(q_z=0)$ are bounded by the frequencies ω_{-m}^c and ω_{+m}^c from branches $-m$ and $+m$, respectively, corresponding to the solution of Eq. (9) with $a_i^- = \pm a_i^+$

$$\sin\left(\frac{\omega(t_2+t_1)}{2}\right) = \pm\,\varepsilon\,\sin\left(\frac{\omega(t_2-t_1)}{2}\right). \tag{10}$$

From Eq. (10) one can notice that the gaps disappear (i) when $\varepsilon=0$, i.e., for the two acoustic impedances being the same or (ii) the phase traversal times $t_i = d_i/v_i$ are the same for both layers. Thus [from Eq. (10)] the mth zone-center frequencies degenerate to

$$\omega_m^c = 2m\pi\frac{v}{d} \quad \text{with} \quad m = 0, \pm 1, \pm 2, \pm 3, \ldots \tag{11}$$

If the magnitude $|\Delta\omega_m^c|$ of the mth zone-center gap is small compared to ω_m^c, as is generally the case, an approximate solution of Eq. (10) can be assumed to be located symmetrically around ω_m^c, i.e., $\omega_{\pm m}^c = \omega_m^c \pm \Delta\omega_m^c/2$. Since the right-hand side of Eq. (10) is a slowly varying function of ω, it can be replaced by ω_m^c. By expanding the left-hand side of Eq. (10) around ω_m^c, one can obtain

$$\frac{\Delta\omega_m^c}{2\omega_m^c} \approx \pm\frac{1}{m\pi}(-1)^m\varepsilon\,\sin\left[m\pi\frac{(t_2-t_1)}{(t_2+t_1)}\right]$$

or

$$\frac{\Delta\omega_m^c}{2} \approx \frac{2v}{d}\left|\varepsilon\,\sin\left[m\pi\frac{(1-\alpha)v_2-\alpha v_1}{(1-\alpha)v_2+\alpha v_1}\right]\right| \quad \text{with} \quad \alpha = d_2/d. \tag{12}$$

One can note that the magnitude of the zone-center gap $\Delta\omega_m^c$ which is comparable for all m on the assumption of a linear dispersion, displays an oscillatory behavior as a function of α and is proportional to the modulation parameter ε, to the averaged velocity v, and is inversely proportional to the SL period d.

B. Zone-boundary gaps

Following the procedure outlined above, one can calculate the frequency gaps at the zone boundary of the SL Brillouin zone by setting $q_z = \pi/d$. As the mth gap at the zone boundary is delimited by ω_m^b and $\omega_{-(m+1)}^b$ the two frequencies become the solutions of Eq. (9) with $q_z = \pi/d$ and $a_i^- = a_i^+$

$$\cos\left(\frac{\omega(t_2+t_1)}{2}\right) = \pm\,\varepsilon\,\cos\left(\frac{\omega(t_2-t_1)}{2}\right), \tag{13}$$

and the mth gap is located around $\omega_m^b = |2m+1|\pi/(t_1+t_2)$ with $m=0,\pm 1,\pm 2,\ldots$ Assuming once again that the magnitude of the frequency gap $|\Delta\omega_m^b| = \omega_{-(m+1)}^b - \omega_m^b$ is much smaller than ω_m^b one can derive

$$\frac{\Delta\omega_m^b}{2} \approx \frac{2v}{d}\left|\varepsilon\,\cos\left[\frac{|2m+1|\pi}{2}\frac{(1-\alpha)v_2-\alpha v_1}{(1-\alpha)v_2+\alpha v_1}\right]\right|$$

$$\text{with} \quad \alpha = d_2/d. \tag{14}$$

IV. NUMERICAL COMPUTATIONS, RESULTS, AND DISCUSSIONS

A. Phonon dispersions of BeS, BeSe, and BeTe

In semiconductors the behavior of phonon dispersions reflects specific features about their crystalline structure as well as interatomic forces that bind the materials' atoms together and, therefore, offers the most comprehensive and detailed information about their dynamical behavior. In the harmonic approximation using a rigid-ion model, the existing neutron-scattering data[58,59] of phonon dispersions in Zn chalcogenides have provided us with a very good account[74] of the interatomic interactions. Recent first-principle studies of first-order elastic constants, bulk modulii,[37] and phonon frequencies[39] at high-symmetry points in BeS, BeSe, and BeTe were useful (see Table II) for us in constructing an optimized rigid-ion model following the procedures developed elsewhere.[61] The main reason for choosing the current lattice dynamical scheme is its simplicity that allowed us to analyze the vibrational properties of both the bulk Be-Zn chalcogenide materials and their SLs. The perusal of Table I reveals that as compared to Zn chalcogenides[74] the short-range force constants in BeS, BeSe, and BeTe are much stronger with lower values for the effective (Z_{eff}) charges. We find these results to be consistent with an earlier first-principles study[8] which predicted an increase in the covalency and higher strength between the Be-A bonds as compared to the bonding between Zn-A (where A=S, Se, and Te). In this respect, we also noticed some similarities between Be chalcogenides and B pnictides[62] (BP, BAs, and BSb), III-Ns (Ref. 63) (AlN, GaN, and InN), and β SiC.[69]

The calculated phonon-dispersion curves along high-symmetry directions, one-phonon density of states, and Debye temperatures are presented in Figs. 2–4, respectively, for Zn and Be chalcogenides using parameter values of Table I. In Zn-chacogenides, the phonon frequencies [see Figs. 2(a)–2(c)] at critical points are found to be in very good agreement with the existing, optical (Raman, IR) and inelastic neutron scattering[58,59] data. From our study we noticed decrease in the zone-center optical [LO(Γ) and TO(Γ)] mode frequencies with the increase of anion mass in the XS, XSe, and XTe, with X=Be,Zn, sequences. In Be chalcogenides, although the calculated values of the zone-center LO(Γ), TO(Γ) mode frequencies are in good agreement with the experimentally determined (Raman and IR) data we noticed, however, quite unusual characteristics [see Figs. 3(a)–3(c)] in the optical phonon dispersions along Γ-X (001) and Γ-L (111) directions when compared with several II-VI and III-V compounds with similar crystal structure. For instance, (i) the LO, TO branches along high-symmetry directions ($\Gamma \rightarrow X$ and $\Gamma \rightarrow L$) are nearly dispersionless; (ii) the values of the TO modes are significantly lower than that of the LO modes; and (iii) the difference between LO(Γ)-TO(Γ) frequencies decrease from BeS→BeSe→BeTe and the separations between optical and acoustical modes increase. These behaviors can be correlated to the large mass difference between Be and chalcogen (S, Se, and Te) atoms and to the decrease in the material's bond polarity α_p (Ref. 75) (see Table IV). Earlier, we found similar atypical features in the phonon dispersions of B pnictides, III-Ns, and β SiC.[62,63,69] We suspect such distinctiveness in the dynamical characteristics linked, most likely, to the lighter masses and radically different covalent radii of Be, B, N, and C, in Be chalcogenides, B pnictides, III-Ns, and IV-Cs, respectively. In the absence of acoustical (LA) phonons at the edge of the Brillouin zone our lattice dynamical calculations in Be chalcogenides fall well within the upper limits obtained[54] from the longest wave vectors and sound velocities $\{q_m \nu_{\text{LA}}/(2\pi c)\}$. For BeSe our calculated LA phonon value compares favorably with the frequency derived by the first-principles calculation in the Be-rich supercell configurations.[52] Moreover, in the framework of a linear diatomic chain model, the widths of the frequency ranges for the acoustic, optical, and optical-acoustic modes are seen to vary approximately as $(1/\sqrt{m_X})$, $(\sqrt{1+m_{\text{Be}}/m_X}-1)$, and $(1-\sqrt{m_{\text{Be}}/m_X})$, respectively (cf. Table IV), with m_{Be} and m_X (X=S, Se, and Te) being the masses of Be and chalcogen atoms. Again, the results of rigid-ion model calculations for optical phonons in Be-Zn chalcogenides along with the Green's function calculations (unpublished) of impurity modes in BeX:Zn (ZnX:Be) have (cf. Sec. IV C) played a significant role in understanding the observed phonon mode behaviors in ternary Be-Zn chalcogenides.

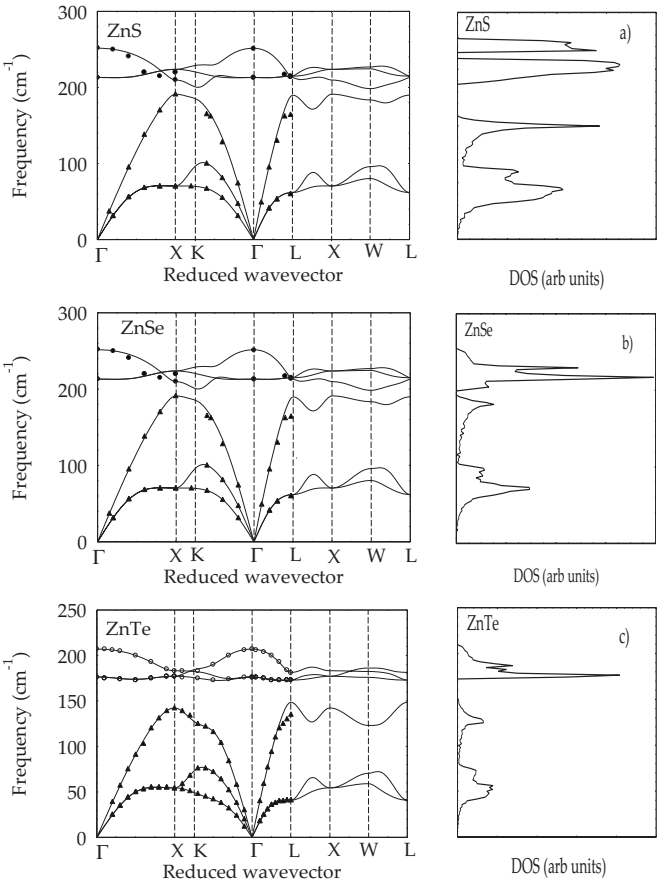

FIG. 2. Experimental (▲●○) (Refs. 58 and 59) and calculated (solid lines) phonon-dispersion curves along high-symmetry directions based on our rigid-ion model (Ref. 74) along high-symmetry directions and one-phonon density of states for (a) ZnS, (b) ZnSe, and (c) ZnTe.

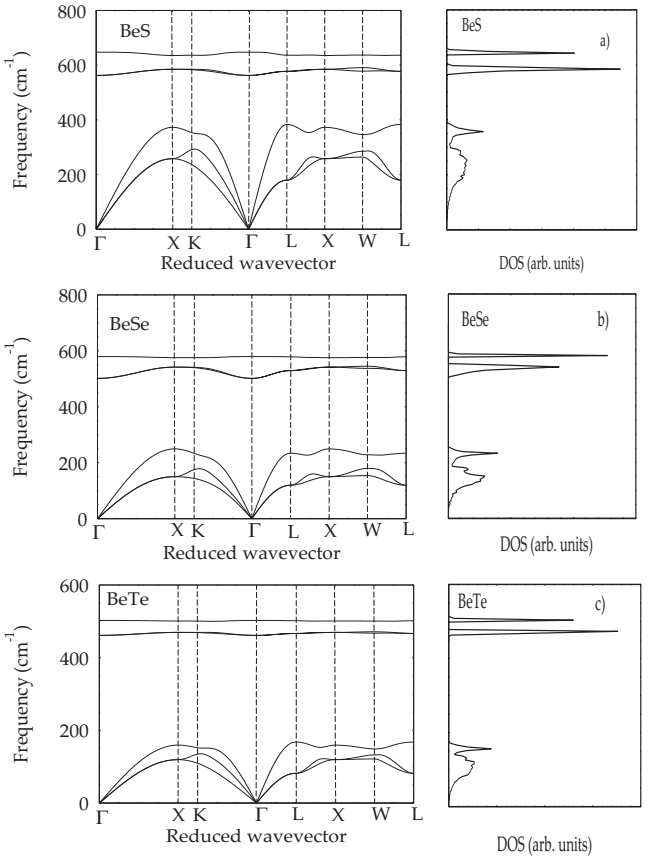

FIG. 3. Calculated (solid lines) phonon-dispersion curves along high-symmetry directions based on our rigid-ion model and using the set of parameters given in Table I along high-symmetry directions and one-phonon density of states for (a) BeS, (b) BeSe, and (c) BeTe.

By incorporating phonon energies derived from the rigid-ion model within the quasiharmonic approximation we have calculated the Debye temperatures for Be chalcogenides. One must note that θ_D is a fundamental physical property used to distinguish between high- and low-temperature regions for a solid. In Figs. 4(a)–4(c) we have displayed our lattice dynamical calculations of $\theta_D(T)$ and compared the results for the values of θ_D near $T \rightarrow 0$, and θ_D(min) in Table IV against the limited experimental/theoretical[43,44] data available in the literature.

B. Phonons in SLs

Our rigid-ion model calculations for the optical phonons at the zone center as a function of θ in $(\mathrm{BeSe})_m/(\mathrm{ZnSe})_n$ ($m=n$ for 2 and 3) SLs have exhibited [see Figs. 5(a) and 5(b)] some interesting results. One must note that the angle θ varies from 0 to $\pi/2$ as $\vec{q}$ goes from [001] to [100] in a plane normal to [010]. Although the optical branches of the SLs are well separated ($\sim$500–580 cm^{-1}) for the BeSe-like from the ZnSe-like ($\sim$213–252 cm^{-1}) modes, the polarization of certain zone-center optical modes changes significantly with the propagation direction, clearly indicating an anisotropic behavior. Near $\theta \rightarrow 0$, the symbols LO_n and TO_n designate the nth-quantized phonons derived from the bulk BeSe and ZnSe

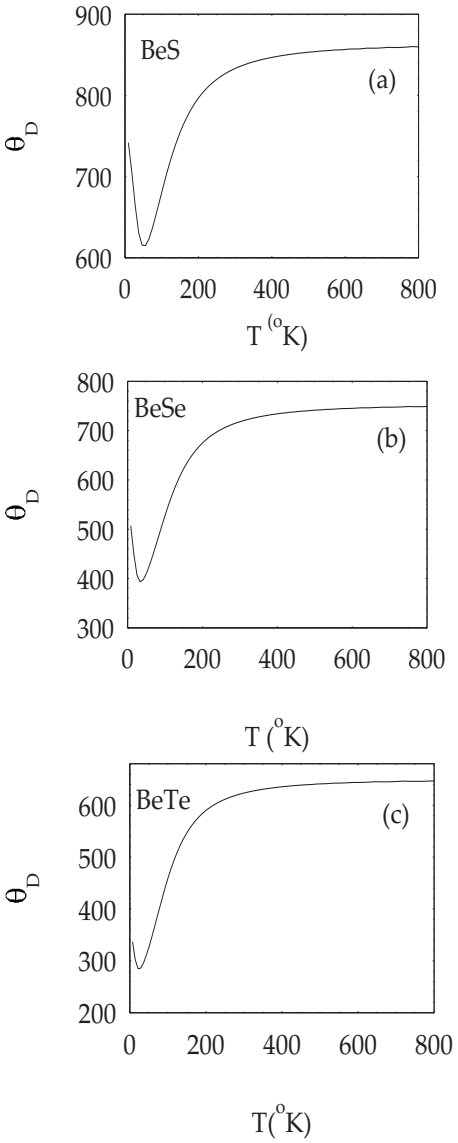

FIG. 4. Calculated Debye temperature θ_D as afunction of T based on our rigid-ion model and using the set of parameters given in Table I for (a) BeS, (b) BeSe, and (c) BeTe.

LO and TO branches. Based on group theoretical arguments, we find that the modes polarized parallel to the layer normal ($\theta=0$) have A_1 or B_2 symmetry and the modes polarized perpendicular to it ($\theta=\pi/2$) have E (twofold) symmetry. As stated in Sec. II B, we noticed [see Figs. 5(a) and 5(b)] that the antisymmetric optic modes exhibit strong angular dependence. Previously, this phenomenon of angular dependence of optical phonons observed experimentally in GaAs/AlAs (Ref. 76) SLs was interpreted in terms of Rytov's macroscopic theory. From the microscopic[73] point of view, we find that the anisotropic behavior is a combined result of the long-range Coulomb interaction and the lack of rotational symmetry. Another interesting point to note from Fig. 5(a) is the fact that in the (2×2) SL (say), while the difference between LO_1, LO_2 BeSe-like confined optical phonons (COPs) is smaller ($\sim$2 cm^{-1}) it is much larger (23 cm^{-1}) for the ZnSe-like COP modes. Similar to GaAs/AlAs SL, the two highest optical frequencies in $(\mathrm{BeSe})_2/(\mathrm{ZnSe})_2$ SL [see

TABLE IV. Comparison of the calculated phonon frequencies (in wave numbers) at the high-symmetry critical points and Debye temperatures (in K) with the existing experimental and theoretical data for BeS, BeSe, and BeTe.

Material properties	BeS		BeSe		BeTe	
	Others	Our	Others	Our	Others	Our
LO(Γ)	647[a]	647	579,[b] 556[a]	579	502[a]	502
TO(Γ)	562[a]	562	501.3,[b] 501[a]	501	461[a]	461
			498,[a] 496		477[b]	
LO(X)	652[a]	635	528,[b] 601[a]	575	468,[b] 540[a]	501
TO(X)	507[a]	585	496,[b] 451[a]	540	477,[b] 425[a]	470
LA(X)	364[a]	372	252,[b] 218[a]	244	140,[b] 159[a]	159
TA(X)	237[a]	258	101,[b] 139[a]	148	80,[b] 97[a]	119
LO(L)	607[a]	636	538,[b] 556[a]	579	481,[b] 504[a]	502
TO(L)	543[a]	577	517,[b] 485[a]	529	473,[b] 455[a]	467
LA(L)	362[a]	383	177,[b] 216[a]	234	74,[b] 158[a]	168
TA(L)	161[a]	179	72,[b] 99[a]	120	67,[b] 69[a]	82
Θ_D(min)	628[c]	615	399,[c] 408[d]	394	289[c]	285
$\Theta_D(T\rightarrow 0)$		742		507		337
α_p		0.63		0.62		0.61

[a]Reference 39.
[b]References 45 and 46.
[c]Reference 43.
[d]Reference 44.

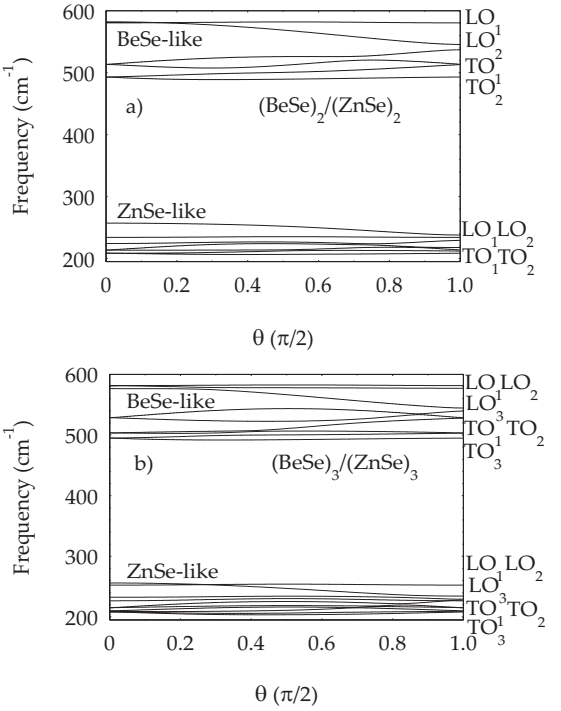

FIG. 5. Calculated dispersions based on our rigid-ion model of long-wavelength ($\boldsymbol{q}=0$) BeSe-like and ZnSe-like optical modes for $(BeSe)_n/(ZnSe)_n$ with (a) $n=2$ and (b) $n=3$ superlattices.

Fig. 5(a)] show the expected LO_1, LO_2 BeSe-like LO modes (with a small energy difference) confined to the BeSe layer. Although no Raman-scattering data exist for the confined optical phonons in BeSe/ZnSe SLs, the energy difference found for the ZnSe-like optical phonons in BeTe/ZnSe SLs (Ref. 60) falls well within the range of our calculations. Similar to $(BeSe)_m/(ZnSe)_n$ SLs, we have earlier observed an analogous confinement of optical phonons in $(AlAs)_m/(GaAs)_n$ SLs by using Raman-scattering spectroscopy.[73] It is worth mentioning that these phonon confinement effects are sensitive not only to the average layer thickness and structural perfection but also to the interface roughness.

C. Folded acoustic phonons

Among the three Be chalcogenides, BeTe is the closely matched to ZnSe which provides excellent opportunities of growing high-quality $(BeTe)_m/(ZnSe)_n$ SLs on GaAs substrates. Earlier, Walter *et al.*[6] had grown BeTe/ZnSe SL samples of 75–100 periods on GaAs (001) at 300 °C by using MBE and deliberately maintaining either the Zn-Te or Be-Se interface. The folded acoustic phonons (FAPs) observed by Raman scattering[56] in two of their samples #1 $(BeTe)_{7.5}/(ZnSe)_{11.5}$ and #3 $(BeTe)_{8.5}/(ZnSe)_{9.5}$ with Zn-Te interfaces indicated a well-defined lateral and in-depth homogeneity of the layer thickness. A half integer of the number of monolayer in these samples accounted for the additional atomic monolayer for the achievement of the desired interface. In the Raman-scattering experiments q_z in Eq. (6) is given by

$$q_z = \frac{4\pi n}{\lambda}\sin\left(\frac{\theta_o}{2}\right), \tag{15}$$

where n is the refractive index of the material, θ_o is the scattering angle, and λ is the wavelength of the incident laser light. By varying λ and θ_o the phonon-dispersion curves can be scanned. Consequently, the doublets detected near 25–30 cm^{-1} in the $z(xx)\bar{z}$ scattering geometry are related to the LA modes due to mini-zone-folding effect. To describe the long-wavelength acoustic phonons, the SL is considered [cf. Eq. (6)] as an elastic continuum where the two alternating layers are characterized by their bulk densities ρ_1, ρ_2, layer thicknesses d_1, d_2, and sound velocities v_1, v_2. From Eq. (6), one can also notice that the dispersion curves of the average bulk material is folded into the new Brillouin zone, in addition, small gaps open up at the zone center and at the boundary for $\zeta\neq 0$. Theoretical results of the zone-folding effects, the creation of mini gaps in the acoustical phonons and the frequencies of the doublet $\omega_{\pm m}$ (marked by X) for $(BeTe)_m/(ZnSe)_n$ SLs shown in Fig. 6 (see Table V) are found to be in very good agreement with the Raman[56] data. One can note that the frequency of the FAP is very sensitive to the thickness of the SL period d_{SL}—a decrease of d_{SL} causes a shift of the FAP to higher frequency.

For BeTe/ZnSe SL we used Eqs. (12) and (14) and calculated the variations of the two lowest acoustic gaps as a function of the relative thickness ratio α at the zone center ($m>0$) and zone edge ($m<0$) normalized to the correspond-

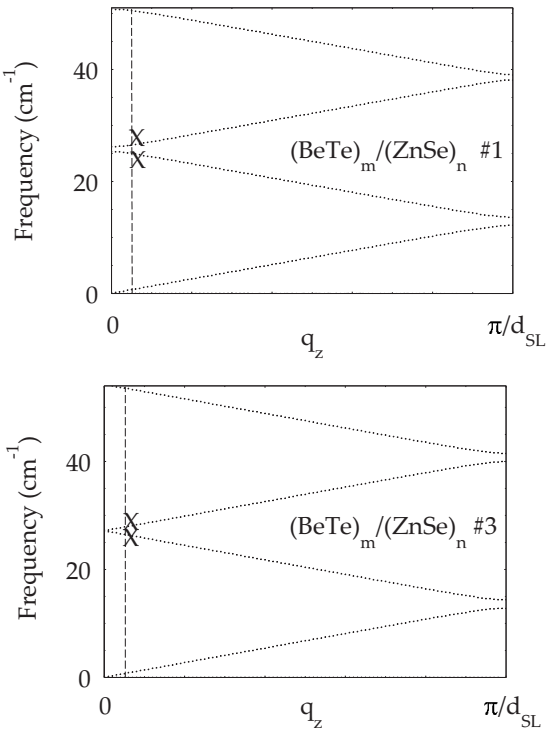

FIG. 6. Calculated dispersion curves based on elastic continuum model for the folded acoustic branches of BeTe/ZnSe SL samples (#1 and #3 see text and Table V) with Raman-scattering data of the observed doublets (X).

ing average frequency. The results displayed in Fig. 7 reveal that the magnitude of the zone-center gap $\Delta\omega_m^c$ which is comparable for all m on the assumption that a linear dispersion exhibits an oscillatory behavior as a function of α and is proportional to the modulation parameter ε, to the averaged velocity v and is inversely proportional to the SL period d. Note that all the zone-center gaps vanish for the same value of $\alpha_c = v_2/(v_1+v_2)$.

D. Phonons in BeZn(Mg)Se(Te) mixed alloys

The Be-based II-VI ternary compounds such as Be_xZn_{1-x} (Mn_{1-x} or Mg_{1-x})Se(Te) are known to display zinc-blende structure for the entire composition range. In $A_xB_{1-x}C$ (with

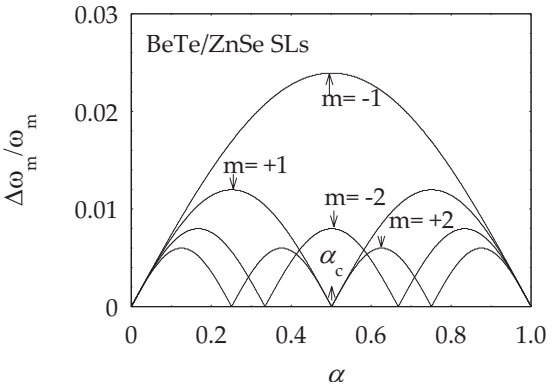

FIG. 7. Elastic continuum model-based calculated acoustical gaps in a BeTe/ZnSe SL at the lower zone center ($m>0$) and zone edge ($m<0$), normalized to the corresponding average frequency as a function of the relative thickness α (see text).

A=Zn, B=Be, Mn, or Mg, and C=Se or Te) alloys, the variation of the zone-center ($\vec{q}=0$) LO and TO phonons with composition x for the binary compounds AC and BC can be identified by using either infrared (IR) and/or Raman-scattering spectroscopies.[7,49–60] Raman scattering has the potential to yield important information about the ternary compounds on a scale on the order of a few lattice constants—it can be used to study the microscopic nature of structural or topological disorder in materials. As mentioned before the "cation-anion" bond lengths (A-C,B-C) in most $A_xB_{1-x}C$ alloys are conserved over the entire composition range x, i.e., the bond lengths of the parent binary (AC,BC) compounds are normally retained. However, due to large variations in the covalent radii between Be (0.85 Å) and Zn (1.22 Å) [or Mn (1.19 Å) or Mg (1.27 Å)], one can question whether the bond lengths Be-Se(Te) and Zn-Se(Te) [or Mn-Se(Te) or Mg-Se(Te)] in the ternary $Be_xZn_{1-x}Se(Te)$ [or $Be_xMn_{1-x}Se(Te)$ or $Be_xMg_{1-x}Se(Te)$] alloys are sustained or not over the entire composition range x. As the physical properties of Be-Zn (Mg or Mn) chalocogenide alloys are strongly dependent on the cation-anion bond lengths (or bond strengths) the large deviations in the covalent radii of Be and Zn (Mg or Mn) are expected to significantly influence their dynamical behavior. In the Be-based ternary alloys, the existing Raman[49,50,54,55,77–79] spectra has not only provided useful information about the phonon mode behav-

TABLE V. Comparison of the calculated (our) and experimental Ref. 56 FAPs (in wave numbers) of $(BeTe)_m/(ZnSe)_n$ SLs. Values in square brackets are from x-ray diffraction measurements.

Material characteristics	Sample #1	Sample #3
m/n	7.5/11.5	8.5/9.5
Interface type	Zn-Te	Zn-Te
ω_{-1}/ω_{+1}(expt.:cm^{-1})	24.06/27.34	25.63/28.64
ω_{-1}/ω_{+1}(calc.:cm^{-1})	25.0/26.50	26.5/27.9
ω_1(expt.:cm^{-1})	25.70	27.14
ω_1(calc.:cm^{-1})	25.75	27.2
d_{SL} (Å)	54.45 [52]	51.56 [48.0]
d_{BeTe}/d_{ZnSe} (Å)	21.86/32.59 [19.07/29.21]	24.64/26.92 [23.21/24.80]

ior with compositional disorder, shifts in the phonon frequency, change of phonon linewidths, asymmetry, etc. but also about the possibility of the existence of local arrangements of different types of bonds.

Earlier, Weise[77] performed the Raman-scattering studies of phonons on a series of $Be_xZn_{1-x}Se/GaAs(001)$ $(0<x<1)$ MBE-grown thin films in the $\bar{z}(x,x)z$ configuration. In Be-rich samples of $x=0.81,0.46$, most of the observed Raman features were attributed to the second-order scattering by the GaAs phonons as the exciting energy employed in this study was below the energy gaps (E_g) of epilayers and hence were transparent to the laser. The phonon features observed in the Raman-scattering configuration $\bar{z}(y,x)z$ employed in the Zn-rich samples of $x=0.09,0.70$, however, revealed both ZnSe-like and BeSe-like LO modes. By using IR spectroscopy Geurts *et al.*[78] were able to obtain zone-center TO phonons as a function of x on the $Be_xZn_{1-x}Se/GaAs(001)$ samples used by Weise in Ref. 77. Similar studies of the optical phonons in $Be_xMg_{1-x}Se/GaAs(001)$ $(0<x\leq 0.4)$ were also reported by Weber.[79] As illustrated in Figs. 8(a)–8(c) the results of zone-center optical phonons from Raman and IR spectroscopy for the $Be_xMg_{1-x}Se$ (Ref. 79) and $Be_xZn_{1-x}Se$ (Refs. 77, 78, and 80) epilayers have exhibited qualitatively the two-phonon mode behavior.

In our study of using MREI scheme we represented the long-wavelength optical phonons of ions in the mixed ternary crystals by their motion in a pseudounit cell. For different values of x, the zone-center optical phonons in these compounds studied by Raman-scattering spectroscopy has exhibited at first sight the two-mode behaviors. By using the set of optimized MREI model parameters, we have displayed in Fig. 8 the results of our calculations for the optical phonons in three ternary alloys BeMgSe, BeZnTe, and BeZnSe, respectively. The comparison of calculated optical phonons with the two-mode behavior observed by Raman-scattering experiments clearly suggest that the present study provides a qualitative description of the ternary alloys. Due to oversimplified assumptions made in the MREI scheme, the calculated values of impurity modes (local or gap) at the limiting values of composition are found to be slightly different from the measured ones. Moreover, the model was unable to account for the TO, LO doublets observed recently in ternary $Be_xZn_{1-x}Se(Te)$ alloys below at intermediate composition range $(\sim 0.2<x\leq 0.9)$.[49,50,54,55] To explain the atypical Raman data of optical phonons in $Be_xZn_{1-x}Se(Te)$ alloys Pagès *et al.*[49,50] used a percolation scheme and have argued that the alloys need to be regarded as composites rather than as uniform continua believed in the VCA-based MREI model. The authors of Ref. 49 have reasoned that due to different mechanical properties of the two host media, the Be-Se(Te) bonds from each of them vibrate at two separate frequencies below the percolation threshold x_c. Similar implication of the ordering of Be-Se bonds in $Be_xZn_{1-x}Se$ alloys was made earlier[57] on the basis of IR and Raman measurements of the optical phonons. It is worth mentioning that all of these characteristics are clearly driven by the addition of Be atoms which not only induces topological disorder but also structural disorder. For allowed phonons these disorders result in the breaking of the dynamical symmetry, leading to

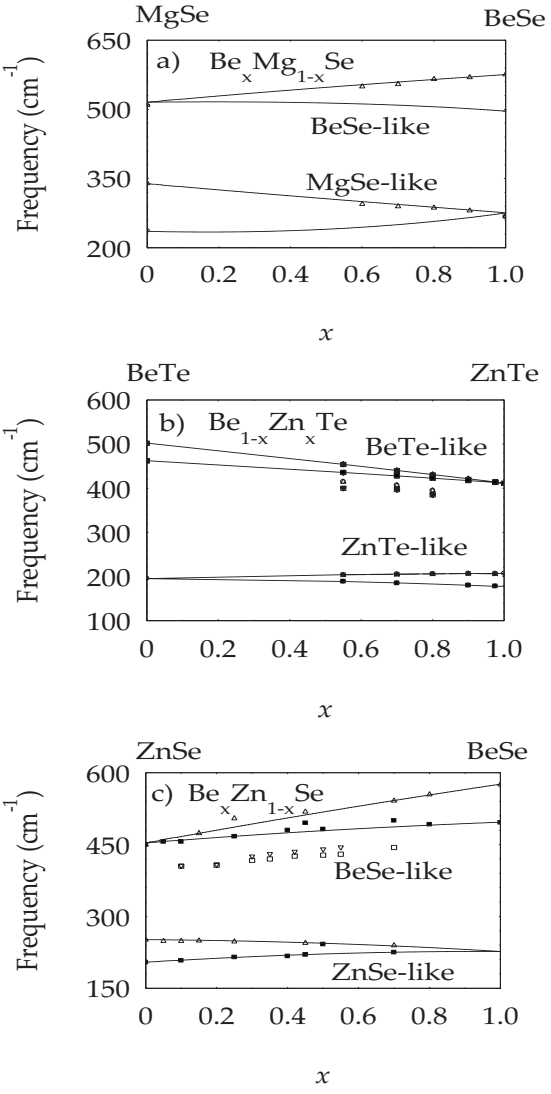

FIG. 8. Calculated variations of the observed Raman-scattering data (Refs. 77–79) of LO and TO frequencies for the ternary (a) $Be_xMg_{1-x}Se$, (b) $Be_{1-x}Zn_xTe$, and (c) and $Be_xZn_{1-x}Se$ compounds as a function of composition x based on the MREI model using the set of parameters of Table III. Solid lines are the best fits to the experimental data (symbols). One can notice that the extra doublets observed in Raman spectroscopy (Refs. 49 and 50) in $Be_{1-x}Zn_xTe$ and $Be_xZn_{1-x}Se$ ternary alloys above the critical values of x cannot be explained by the MREI model (please see text).

the contribution of $\vec{q}\neq 0$ phonons to broaden the Raman line shapes. The broadening of linewidths and asymmetry in ternary alloys can be investigated in terms of the spatial correlation models[81–83] based on finite correlation length of propagating phonon due to the alloy potential fluctuations. Our Green's function theory has also provided (unpublished) a compelling illustration of the disorder-activated vibrational modes in Be-based alloys. Here, we have reported the results of a quantitative analysis of the IR reflectivity (cf. Sec. IV E) at an oblique incidence in $Be_xZn_{1-x}Se/GaAs(001)$ epilayers by using appropriate dielectric functions and incorporating two types of BeSe and one ZnSe modes[54,55,57] following a standard methodology of multilayer optics.[66]

E. IR reflectance study in ternary alloys and thin epilayers

While Raman-scattering spectroscopy[7,49–57] is a highly sensitive technique for studying the phonons in II-VI semiconductor alloys, many researchers have relied on using far-infrared reflectance[30–33,57,60,84] for characterizing thin films, quantum wells, SLs, and nanostructured materials by studying their dynamical properties. In recent years, several far-infrared studies of optical phonons in ternary alloys $Zn_{1-x}Mn_xTe$ (Ref. 84) $(0<x<0.15)$, $Zn_{1-x}Mn_xSe$ (Ref. 82) $(0<x<0.29)$, and $Be_xZn_{1-x}Se/GaAs(001)$ (Ref. 57) have been reported. The Mn composition dependence of optical phonons in $Zn_{1-x}Mn_xTe$ (Ref. 84) has displayed an intermediate phonon mode behavior between one- and two-mode types. Similar to the Raman-scattering studies of Pagès *et al.*,[49,50,54,55] the IR measurement[57] provided additional support for the existence of three polar optical phonon modes in MBE-grown $Be_xZn_{1-x}Se/GaAs(001)$ $(0\leq x\leq 1, 0.3-1\ \mu m)$ alloy system—signifying the possibility of two types of Be-Se bonds (ordering) and one type of Zn-Se bond appearing in the frequency range of $400-575\ cm^{-1}$ and $200-250\ cm^{-1}$, respectively.

To understand the IR spectra, we have performed a quantitative analysis for the reflectivity of a 0.5-μm-thick $Be_xZn_{1-x}Se/GaAs(001)$ $(x=0.81)$ epilayer at an oblique incidence $(\theta=40°)$ by numerically calculating the necessary complex dielectric functions $\tilde{\varepsilon}(\omega)$ and using the standard methodology of multilayer optics. In order to describe the optical properties of thin films grown on a substrate, one needs to consider three medium, i.e., (i) the vacuum with dielectric function $[\tilde{\varepsilon}_1(\omega)]$ for the incidence light beam of wavelength λ, (ii) the dielectric function $\tilde{\varepsilon}_2(\omega)$ of the binary or ternary layer with thickness d, and (iii) the dielectric function of the substrate $\tilde{\varepsilon}_3(\omega)$ on which the epilayer is grown. It is straightforward to obtain the amplitude of the reflection coefficient $\tilde{r}_{123}$ or the reflectivity $R(\omega)=|\tilde{r}_{123}|^2$ in a normal incidence by using

$$\tilde{r}_{123}=\frac{\tilde{r}_{12}+\tilde{r}_{23}\exp(2i\beta)}{1+\tilde{r}_{12}\tilde{r}_{23}\exp(2i\beta)}, \tag{16}$$

where $\tilde{r}_{12}=(\frac{1-\tilde{n}_2}{1+\tilde{n}_2})$; $\tilde{r}_{23}=(\frac{\tilde{n}_2-\tilde{n}_3}{\tilde{n}_2+\tilde{n}_3})$ with $\tilde{n}_2=\sqrt{\tilde{\varepsilon}_2(\omega)}$ and $\tilde{n}_3=\sqrt{\tilde{\varepsilon}_3(\omega)}$ being the Fresnel coefficients. The term $\beta[=2\pi d\frac{\sqrt{\tilde{\varepsilon}_2(\omega)}}{\lambda}]$ in Eq. (16) is the phase multiplier and λ is the wavelength. The formulation of reflectivity for an oblique incidence is a little more involved.[66] We have calculated the dielectric functions of the material samples by using the Lorentz multioscillator scheme by expressing $\tilde{\varepsilon}(\omega)$ as a sum of the contributions from the lattice vibrations or phonons

$$\tilde{\varepsilon}(\omega)=\varepsilon_\infty+\sum_j\frac{S_j\omega_{TOj}^2}{\omega_{TOj}^2-\omega^2-i\omega\Gamma_j}. \tag{17}$$

In Eq. (17) the value ε_∞ represents the high-frequency dielectric constant; S_j is the oscillator strength; ω_{TOj} and Γ_j are, respectively, the resonance frequency and damping parameters of the jth TO phonon.

In simulating the reflectivity at an oblique incidence $(\theta=40°)$ of the $Zn_{1-x}Be_xSe/GaAs(001)$ epifilm $(x=0.81)$ we used a three-oscillator [i.e., *one* (Zn-Se), and *two* (Be-Se)] version of the Lorentz model with optical phonon frequencies $(j=1,2,3;\ \omega_{TO1}=213.0,\ \omega_{TO2}=478.0\ cm^{-1},\ \omega_{TO3}=499.0\ cm^{-1})$ derived from the Raman-scattering data. The oscillator strengths S_j and damping constants Γ_j of the jth ω_{TOj} were attuned to accomplish the best fit between theoretical and experimental (see Fig. 9) data. The results of our analysis have provided strong justification to the fact that for a critical value of x_c in $Zn_{1-x}Be_xSe$ there exist at least two types of Be-Se bonds (2a, 2b) with optical mode frequencies between $400-575\ cm^{-1}$ involving two kinds of local atomic arrangements.

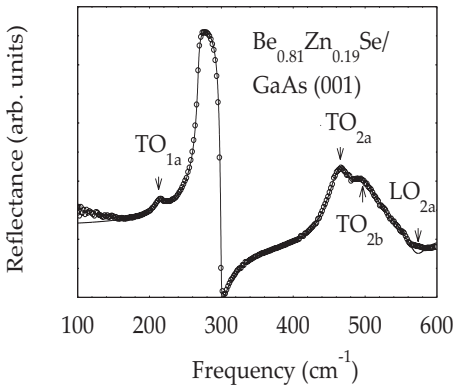

FIG. 9. Comparison of the experimental (○) and theoretical (—) results for the IR spectra of $Be_{0.81}Zn_{0.19}Se$, 0.5-μm-thick epilayer grown on GaAs (001) at 40° oblique incidence using a damped three Lorentzian-oscillator model (please see text).

V. CONCLUSIONS

In conclusion, we have performed and reported the results of a comprehensive study of the optical and vibrational properties of Be-Zn chalcogenides, ternary alloys, and superlattices by using a realistic lattice dynamical model. For beryllium compounds (BeS, BeSe, and BeTe) although the calculated zone-center phonons are in good agreement with the existing experimental data we noticed, however, atypical characteristics in the optical phonon dispersions along Γ-X and Γ-L symmetry directions after comparing them with other II-VI compounds of similar crystal structure. These unusual dynamical properties caused by the increase in materials' bond strength and decrease in the bond polarity are related to the large mass difference and the covalent radii of Be and chalcogen atoms. In the quasiharmonic approximation our lattice dynamical results of $\theta_D(T)$ for Be chalcogenides compared very well with the limited experimental/theoretical[43,44] data available in the literature. Similar to $(AlAs)_m/(GaAs)_n$ (Ref. 76) the polarization in $(BeSe)_m/(ZnSe)_n$ SLs showed significant variation of the zone-center optical phonons as a function of θ exhibiting anisotropic behavior. In a (2×2) SL we have noticed that while the difference between LO_1, LO_2 BeSe-like COPs is smaller $\sim 2\ cm^{-1}$ it is much larger $23\ cm^{-1}$ for the ZnSe-like modes. Although, no Raman-scattering data exist in the literature for the COPs in BeSe/ZnSe SLs—the phonon energy difference found for the ZnSe-like optical phonons in

BeTe/ZnSe SLs (Ref. 60) falls well within the range of our calculations. In earlier studies[76] the angular dependence of optical phonons in SLs was interpreted in terms of the Rytov's macroscopic theory. However, based on our realistic lattice dynamical calculations we find that the anisotropic behavior in SLs is caused by the combined effects of the long-range Coulomb interactions and the lack of rotational symmetry. In terms of an elastic continuum model our results of the zone-folding effects and the creation of mini gaps in the acoustical phonons of $(BeTe)_m/(ZnSe)_n$ SLs are found to be in excellent agreement with the available Raman-scattering data.[56] In order to explain the features observed in the experimental reflectivity of the BeZnSe/GaAs (001) thin film at an oblique incidence we used a damped three-oscillator Lorentz-model and numerically calculated the complex dielectric functions $\tilde{\varepsilon}(\omega)$ by using the standard methodology of multilayer optics. Clearly, our analysis of the IR reflectivity spectra (see Fig. 9) has provided strong corroborations to the fact that in the frequency range of 400–575 cm^{-1} there exist at least two types of Be-Se bonds (2a, 2b) with optical modes involving two different kinds of local atomic arrangements. Although support for the existence of local ordering of Be-chalcogen bonds has been recently proposed[49] using the first-principles calculations—our systematic study for the vibrational properties of Be chalcogenide alloys (unpublished) within the framework of a Green's function theory has also validated this conjecture.

ACKNOWLEDGMENTS

The author wishes to acknowledge the financial support he received from Indiana University of Pennsylvania through its "University Faculty Innovation Grant" and to M. D. Tiwari, Director IIIT, Allahabad, India for a very fruitful discussion on the subject matter.

*talwar@iup.edu

[1] M. W. Cho, S. K. Hong, J. H. Chang, S. Saeki, M. Nakajima, and T. Yao, J. Cryst. Growth **214-215**, 487 (2000).
[2] S. B. Che, I. Nomura, W. Shinozaki, A. Kikuchi, K. Shimomura, and K. Kishino, J. Cryst. Growth **214-215**, 321 (2000).
[3] S. B. Che, I. Nomura, A. Kikuchi, and K. Kishino, Appl. Phys. Lett. **81**, 972 (2002).
[4] A. Waag, F. Fischer, J. J. Lugauer, T. Litz, J. Laubender, U. Lunz, U. Zhender, W. Ossau, T. Gerhardt, M. Moller, and G. Landwehr, J. Appl. Phys. **80**, 792 (1996).
[5] A. Waag, Th. Litz, F. Fischer, H.-J. Lugauer, T. Baron, K. Schüll, U. Zehnder, T. Gerhard, U. Lunz, M. Keim, G. Reuscher, and G. Landwehr, J. Cryst. Growth **184-185**, 1 (1998).
[6] T. Walter, A. Rosenauer, R. Wittmann, D. Gerthsen, F. Fischer, T. Gerhard, A. Waag, G. Landwehr, P. Schunk, and T. Schimmel, Phys. Rev. B **59**, 8114 (1999).
[7] L. Y. Lin, C. W. Chang, W. H. Chen, Y. F. Chen, S. P. Guo, and M. C. Tamargo, Phys. Rev. B **69**, 075204 (2004).
[8] C. Vérié, J. Cryst. Growth **184-185**, 1061 (1998).
[9] S. P. Guo, Y. Luo, W. Lin, O. Maksimov, M. C. Tamargo, I. Kuskovsky, C. Tian, and G. Neumark, J. Cryst. Growth **208**, 205 (2000).
[10] F. Fischer, M. Keller, T. Gerhard, T. Behr, T. Litz, H. J. Lugauer, M. Keim, G. Reuscher, T. Baron, A. Waag, and G. Landwehr, J. Appl. Phys. **84**, 1650 (1998).
[11] T. Yokogawa, S. Yoshii, A. Tsujimura, Y. Sasai, and J. Merz, Jpn. J. Appl. Phys., Part 2 **34**, L751 (1995).
[12] M. Pessa, K. Rakennus, P. Uusimaa, P. Savolainen, and A. Salokatve, Phys. Status Solidi B **187**, 337 (1995).
[13] A. Tsujimura, S. Yoshii, S. Hayashi, K. Ohkawa, and T. Mitsuyu, in *Physical Concepts and Materials for Novel Optoelectronic Device Applications II*, Proc. SPIE Vol. 1985, edited by Fabio Beltram and Erich Gornik (SPIE, 1993), pp. 468–475.
[14] C. Chung, F. Jain, and G. Drake, J. Cryst. Growth **117**, 1062 (1992).
[15] A. Nurmikko and R. L. Gunshore, in *Integrated Photonics Research*, OSA Technical Digest Series Vol. 10 (Optical Society of America, New Orleans, 1992).
[16] I. V. Sedova, S. V. Sorokin, A. A. Sitnikova, R. V. Zolotaveva, S. V. Ivanov, and P. S. Kop'ev, Seventh International Symposia on Nanostructure "Physics and Technology," St. Petersburg, Russia, June 14–18, 1999 (unpublished); http://handle.dtic.mil/100.2/ADP012998
[17] S. V. Ivanov, A. A. Toropov, S. V. Sorokin, T. V. Shubina, N. D. Il'inskaya, A. V. Lebedev, I. V. Sedova, P. S. Kop'ev, Zh. I. Alferov, H.-J. Lugauer, G. Reuscher, M. Keim, F. Fischer, A. Waag, and G. Landwehr, Semiconductors **32**, 1137 (1998).
[18] L. H. Kuo, L. Salamanca-Riba, B. J. Wu, G. M. Haugen, J. M. DePuydt, G. Hofler, and H. Cheng, J. Vac. Sci. Technol. B **13**, 1694 (1995).
[19] L. Worschech, W. Ossau, W. Behr, Th. J. Nurnberger, and G. Landwehr, Appl. Phys. Lett. **73**, 835 (1998).
[20] H. Jeon, J. Ding, A. V. Nurmikko, W. Xie, D. C. Grillo, M. Kobayashi, R. L. Gunshor, G. C. Hua, and N. Otsuka, Appl. Phys. Lett. **60**, 2045 (1992).
[21] M. M. Zverev, D. V. Peregudov, I. V. Sedova, S. V. Sorokin, S. V. Ivanov, and P. S. Kop'ev, Quantum Electron. **34**, 909 (2004).
[22] C. Vérié, in *Semiconductors Heteroepitaxy*, edited by B. Gil and R. L. Aulombard (World Scientific, Singapore, 1995), p. 73.
[23] F. Vigué, E. Tournié, and J. P. Faurie, Appl. Phys. Lett. **76**, 242 (2000).
[24] E. Kato, H. Noguchi, M. Nagai, H. Okuyuma, S. Kijima, and A. Ishibashi, Electron. Lett. **34**, 282 (1998).
[25] D. C. Grillo, M. D. Ringle, G. C. Hua, J. Han, and R. L. Gunshor, J. Vac. Sci. Technol. B **13**, 720 (1995).
[26] X. Zhou, M. C. Tamargo, S. P. Guo, and Y. C. Chen, J. Electron. Mater. **32**, 733 (2003).
[27] Y. Gu, I. L. Kuskovsky, J. Fung, R. Robinson, I. P. Herman, G. F. Neumark, X. Zhou, S. P. Guo, and M. C. Tamargo, Appl. Phys. Lett. **83**, 3779 (2003).
[28] Y. Niiyama and M. Watanabe, Semicond. Sci. Technol. **20**, 1187 (2005); Y. Niiyama, T. Murata, and M. Watanabe, Phys. Status Solidi C **3**, 878 (2006).
[29] F. Vigué, A. Bouillé, E. Tournié, and J.-P. Faurie, Phys. Status

Solidi A **180**, 301 (2000).
[30] M. R. Buckley, F. C. Peiris, O. Maksimov, M. Muñoz, and M. C. Tamargo, Appl. Phys. Lett. **81**, 5156 (2002).
[31] H. Lee, S. Lee, and J. K. Furdyna, Appl. Phys. Lett. **79**, 737 (2001).
[32] A. A. Wronkowska, A. Wronkowski, F. Firszt, and S. Łęgowski, Cryst. Res. Technol. **41**, 580 (2006).
[33] N. Mandal, F. C. Peiris, O. Maksimov, and M. C. Tamargo, Solid State Commun. **149**, 1698 (2009).
[34] H. Lee, I.-Y. Kim, J. Powell, D. E. Aspnes, S. Lee, F. Peiris, and J. K. Furdyna, J. Appl. Phys. **88**, 878 (2000).
[35] C. Chauvet, E. Tournié, P. Vennéguès, and J. P. Faurie, J. Electron. Mater. **29**, 883 (2000); C. Chauvet, E. Tournié, and J. P. Faurie, Phys. Rev. B **61**, 5332 (2000).
[36] O. Maksimov and M. C. Tamargo, Appl. Phys. Lett. **79**, 782 (2001).
[37] M. González-Díaz, P. Rodríguez-Hernández, and A. Muñoz, Phys. Rev. B **55**, 14043 (1997).
[38] C. M. I. Okoye, Eur. Phys. J. B **39**, 5 (2004).
[39] G. P. Srivastava, H. M. Tütüncü, and N. Günhan, Phys. Rev. B **70**, 085206 (2004).
[40] A. Muñoz, P. Rodríguez-Hernández, and A. Mujica, Phys. Status Solidi B **198**, 439 (1996).
[41] D. Heciri, L. Beldi, S. Drablia, H. Meradji, N. E. Derradji, H. Belkhir, and B. Bouhafs, Comput. Mater. Sci. **38**, 609 (2007).
[42] C. Jing, C. Xiang-Rong, Z. Wei, and Z. Jun, Chin. Phys. B **17**, 1377 (2008).
[43] R. P. Singh and R. K. Singh, Appl. Acoust. **71**, 328 (2010).
[44] F. Kong and G. Jiang, Physica B **404**, 3935 (2009).
[45] S. Doyen-Lang, O. Pages, L. Lang, and J. Hugel, Phys. Status Solidi B **229**, 563 (2002).
[46] V. Wagner, S. Gundel, T. Gerhard, Th. Litz, H.-J. Lugauer, F. Fischer, A. Waag, G. Landwehr, R. Kruse, Ch. Becker, and U. Küster, J. Cryst. Growth **184-185**, 1067 (1998).
[47] V. Wagner, J. J. Liang, R. Kruse, S. Gundel, M. Kleim, A. Waag, and J. Geurts, Phys. Status Solidi B **215**, 87 (1999).
[48] J. De Launay, Solid State Phys. **3**, 203 (1957).
[49] O. Pagès, A. V. Postnikov, A. Chafi, D. Bormann, P. Simon, F. Glas, F. Firszt, W. Paszkowicz, and E. Tournié, Eur. Phys. J. B **73**, 461 (2010).
[50] O. Pagès, J. Souhabi, A. V. Postnikov, and A. Chafi, Phys. Rev. B **80**, 035204 (2009).
[51] M. Kozielski, Acta Phys. Pol. A **111**, 343 (2007).
[52] M. Ajjoun, T. Tite, A. Chafi, J. P. Laurenti, O. Pagès, and E. Tournié, J. Alloys Compd. **382**, 271 (2004); A. V. Postnikov, O. Pagès, and J. Hugel, Phys. Rev. B **71**, 115206 (2005).
[53] I. L. Kuskovsky, Y. Gu, J. E. Spanier, I. P. Herman, G. F. Neumark, O. Maksimov, X. Zhou, M. C. Tamargo, V. A. Smyntyna, V. M. Belous, and V. A. Pasternak, J. Phys. Stud. **8**, 384 (2004).
[54] M. Ajjoun, O. Pagès, J. P. Laurenti, D. Bormann, C. Chauvet, E. Tournié, J. P. Faurie, and O. Gorochov, Thin Solid Films **403-404**, 530 (2002); O. Pagès, M. Ajjoun, D. Bormann, C. Chauvet, E. Tournié, J. P. Faurie, and O. Gorochov, J. Appl. Phys. **91**, 9187 (2002); Proceedings of the Tenth International Conference on II-VI Compounds, Bremen, Allemagne (unpublished) [O. Pagès, M. Ajjoun, J. P. Laurenti, D. Bormann, C. Chauvet, E. Tournié, and J. P. Faurie, Phys. Status Solidi B **229**, 25 (2002)]; O. Pagès, M. Ajjoun, J. P. Laurenti, D. Bormann, C. Chauvet, E. Tournié, and J. P. Faurie, Appl. Phys. Lett. **77**, 519 (2000).
[55] O. Pagès, T. Tite, D. Bormann, O. Maksimov, and M. C. Tamargo, Appl. Phys. Lett. **80**, 3081 (2002).
[56] J. J. Liang, Ph.D. thesis, Bayerischen Julius-Maximilians-Universität Würzburg, 2000 and references therein.
[57] A. M. Mintairov, S. Raymond, J. L. Merz, F. C. Peiris, S. Lee, U. Bindley, J. K. Furdyna, V. G. Melehin, and K. Sadchikov, Semiconductors **33**, 1021 (1999).
[58] N. Vagelatos, D. Wehe, and J. S. King, J. Chem. Phys. **60**, 3613 (1974).
[59] B. Hennion, F. Moussa, G. Pepy, and K. Kunc, Phys. Lett. A **36**, 376 (1971).
[60] I. I. Reshina, S. V. Ivanov, V. A. Kosobukin, S. V. Sorokin, and A. A. Toropov, Phys. Solid State **45**, 1579 (2003).
[61] K. Kunc, Ann. Phys. (Paris) **8**, 319 (1973).
[62] D. N. Talwar, G. Thaler, S. Zaranek, K. Peterson, S. Linger, D. Walker, and K. Holliday, Phys. Rev. B **55**, 11293 (1997).
[63] D. N. Talwar, Microelectron. Eng. **43-44**, 309 (1998).
[64] D. N. Talwar, Z. C. Feng, and P. Becla, Phys. Rev. B **48**, 17064 (1993).
[65] M. Rytov, Sov. Phys. Acoust. **2**, 67 (1956).
[66] O. E. Piro, Phys. Rev. B **36**, 3427 (1987).
[67] K. Refson, P. R. Tulip, and S. J. Clark, Phys. Rev. B **73**, 155114 (2006).
[68] P. Pavone, J. Phys.: Condens. Matter **13**, 7593 (2001); R. Jones, Philos. Trans. R. Soc. London **341**, 351 (1992).
[69] D. N. Talwar, in *Dilute III-V Nitride Semiconductors and Material Systems – Physics and Technology*, Springer Series in Materials Science Vol. 105, edited Ayse Erol (Springer-Verlag, Berlin, 2008), Chap. 9, p. 222.
[70] G. Kanellis, Phys. Rev. B **35**, 746 (1987).
[71] I. F. Chang and S. S. Mitra, Phys. Rev. **172**, 924 (1968).
[72] P. V. Santos, L. Ley, J. Mebert, and O. Koblinger, Phys. Rev. B **36**, 4858 (1987).
[73] D. N. Talwar, B. Roughani, J. G. Pellegrino, P. Amirtharaj, and S. B. Qadri, Mater. Sci. Eng., B **44**, 143 (1997).
[74] D. N. Talwar, M. Vandevyver, K. Kunc, and M. Zigone, Phys. Rev. B **24**, 741 (1981).
[75] W. Harrison, *Electronic Structure of Solids* (Dover, New York, 1980).
[76] Yu A. Pusep, A. G. Milekhin, and A. I. Toropov, J. Phys.: Condens. Matter **7**, 1493 (1995).
[77] B. Weise, Diploma thesis, Universität Würzburg, 1998.
[78] J. Geurts, V. Wagner, B. Weise, J. J. Liang, H. Lugauer, A. Waag, L. Landwehr, and R. Kruse, in *Proceedings of the 24th ICPS*, Jerusalem, edited by B. D. Gershoni (World Scientific, Singapore, 1998), p. 1264.
[79] M. Weber, *Schriftliche Hausarbeit der ersten Staatsprüfung für das Lehramt an Gymnasien* (Universität Würzburg, 1999).
[80] H. Ho, K. H. Yoo, M. W. Cho, and T. Yao, J. Korean Phys. Soc. **35**, 92 (1999).
[81] K. K. Tiong, P. M. Amirtharaj, F. H. Pollack, and D. E. Aspnes, Appl. Phys. Lett. **44**, 122 (1984).
[82] P. Parayanthal and F. H. Pollak, Phys. Rev. Lett. **52**, 1822 (1984).
[83] T. R. Yang, C. C. Lu, W. C. Chou, Z. C. Feng, and S. J. Chua, Phys. Rev. B **60**, 16058 (1999).
[84] B. Oleŝ and H. G. von Schnering, J. Phys. C **18**, 6289 (1985).